

NASA/CR-1999-209106
ICASE Report No. 99-14



Solving Upwind-biased Discretizations: Defect-correction Iterations

Boris Diskin
ICASE, Hampton, Virginia

James L. Thomas
NASA Langley Research Center, Hampton, Virginia

Institute for Computer Applications in Science and Engineering
NASA Langley Research Center
Hampton, VA

Operated by Universities Space Research Association



National Aeronautics and
Space Administration

Langley Research Center
Hampton, Virginia 23681-2199

Prepared for Langley Research Center
under Contract NAS1-97046

March 1999

Available from the following:

NASA Center for Aerospace Information (CASI)
7121 Standard Drive
Hanover, MD 21076-1320
(301) 621-0390

National Technical Information Service (NTIS)
5285 Port Royal Road
Springfield, VA 22161-2171
(703) 487-4650

SOLVING UPWIND-BIASED DISCRETIZATIONS: DEFECT-CORRECTION ITERATIONS

BORIS DISKIN* AND JAMES L. THOMAS†

Abstract. This paper considers defect-correction solvers for a second order upwind-biased discretization of the 2D convection equation. The following important features are reported

1. The asymptotic convergence rate is about 0.5 per defect-correction iteration.
2. If the operators involved in defect-correction iterations have different approximation order, then the initial convergence rates may be very slow. The number of iterations required to get into the asymptotic convergence regime might grow on fine grids as a negative power of h . In the case of a second order target operator and a first order driver operator, this number of iterations is roughly proportional to $h^{-1/3}$.
3. If both the operators have the second approximation order, the defect-correction solver demonstrates the asymptotic convergence rate after three iterations at most. The same three iterations are required to converge algebraic error below the truncation error level.

A novel comprehensive half-space Fourier mode analysis (which, by the way, can take into account the influence of discretized outflow boundary conditions as well) for the defect-correction method is developed. This analysis explains many phenomena observed in solving non-elliptic equations and provides a close prediction of the actual solution behavior. It predicts the convergence rate for each iteration and the asymptotic convergence rate. As a result of this analysis, a new very efficient adaptive multigrid algorithm solving the discrete problem to within a given accuracy is proposed. Numerical simulations confirm the accuracy of the analysis and the efficiency of the proposed algorithm. The results of the numerical tests are reported.

Key words. convection, upwind-biased discretization, defect-correction iteration

Subject classification. Applied and Numerical Mathematics

1. Introduction. This is the first in a series of papers analyzing the efficiency of different iterative algorithms solving upwind-biased discretizations of the convection operator. The model problem we study in this paper is the 2D constant coefficient convection equation

$$(1.1) \quad LU \equiv (\bar{a} \cdot \nabla)U = F(x, y),$$

where $\bar{a} = (a_1, a_2)$ is a given vector.

The solution $U(x, y)$ is a differentiable function defined on the unit square $(x, y) \in [0, 1] \times [0, 1]$. In this paper, we deal mostly with the homogeneous equation $F(x, y) \equiv 0$. Exceptions when non-homogeneous right-hand side functions $F(x, y)$ are considered will be emphasized specifically.

*Institute for Computer Applications in Science and Engineering, Mail Stop 403, NASA Langley Research Center, Hampton, Virginia 23681-2199 (email: bdiskin@icase.edu). This research was supported by the National Aeronautics and Space Administration under NASA Contract No. NAS1-97046 while the author was in residence at the Institute for Computer Applications in Science and Engineering (ICASE), NASA Langley Research Center, Hampton, Virginia 23681-2199

†Aerodynamic and Acoustic Methods Branch, Mail stop 128, NASA Langley Research Center, Hampton, VA 23681-2199 (email: j.l.thomas@larc.nasa.gov).

Let ϕ be the non-alignment angle (another name which is common in CFD is the angle of attack), i.e., the angle between the vector \bar{a} and the positive direction of the x axis; $t = \tan \phi = a_2/a_1$ is the non-alignment parameter. For simplicity we assume $a_1 \geq a_2 \geq 0$ and, therefore, $1 \geq t \geq 0$. Then, Eq. (1.1) can be rewritten as

$$(1.2) \quad \partial_\xi U = F(x, y) / \sqrt{a_1^2 + a_2^2},$$

where $\xi = \frac{x+ty}{\sqrt{1+t^2}}$ is a variable along the characteristic of Eq. (1.1).

Eq. (1.1) is supplied with Dirichlet boundary conditions at the inflow boundary $x = 0$ and periodic conditions in the y direction.

$$(1.3) \quad U(0, y) = g(y), \quad U(x, y) = U(x, y + 1),$$

where $g(y)$ is a given function.

This problem is discretized on the 2D Cartesian uniform grid with meshsize h in both the x and y directions. Let u_{i_1, i_2} be a discrete approximation to the solution $U(x, y)$ at the point $(x, y) = (i_1 h, i_2 h)$. Then, the second order accurate discretization corresponding to the Van Leer's scheme with $\kappa = 0$ is defined as

$$(1.4) \quad \begin{aligned} L^h u_{i_1, i_2} &\equiv \frac{1}{4\sqrt{1+t^2}h} \left(\begin{aligned} &(u_{i_1+1, i_2} + 3u_{i_1, i_2} - 5u_{i_1-1, i_2} + u_{i_1-2, i_2}) \\ &+ t(u_{i_1, i_2+1} + 3u_{i_1, i_2} - 5u_{i_1, i_2-1} + u_{i_1, i_2-2}) \end{aligned} \right) = f_{i_1, i_2}; \\ L^h u_{N, i_2} &\equiv \frac{1}{2\sqrt{1+t^2}h} \left(\begin{aligned} &(3u_{N, i_2} - 4u_{N-1, i_2} + u_{N-2, i_2}) \\ &+ t(3u_{N, i_2} - 4u_{N, i_2-1} + u_{N, i_2-2}) \end{aligned} \right) = f_{N, i_2}; \\ i_1 &= 1, 2, \dots, N-1, \quad i_2 = 1, 2, \dots, N, \quad N = 1/h; \\ u_{0, i_2} &= g(i_2 h), \quad u_{-1, i_2} = g'(i_2 h). \end{aligned}$$

In computing L^h at nodes with $i_2 = 1$, $i_2 = 2$, and $i_2 = N$ the vertical periodicity is employed. The outflow boundary conditions at $i_1 = N$ are discretized by the second order upwind scheme. The discretization of the right-hand side function is $f_{i_1, i_2} = F(i_1 h, i_2 h) / \sqrt{a_1^2 + a_2^2}$. Function $g'(y)$ is an additional numerical boundary condition. In model problems where the exact solution $U(x, y)$ is known, one can define $g'(y) = U(-h, y)$.

The discrete scheme (1.4) is upwind biased but not a pure upstream scheme since for defining the operator value at the point (i_1, i_2) , the solution values at the downstream points $(i_1 + 1, i_2)$ and $(i_1, i_2 + 1)$ are required.

1.1. Defect-Correction Schemes. The subject of this paper is the defect-correction method (see [6]) which is widely used to iterate non-upwind discretizations. Let our target discrete problem be

$$(1.5) \quad L^h u_{i_1, i_2} = f_{i_1, i_2},$$

where L^h is a upwind-biased discretization of the convection operator (e.g., (1.4)).

Let L_{st}^h be a stable (say, the first or the second order pure upwind) discretization of the same convection operator and \tilde{u}_{i_1, i_2} be the current solution approximation. Then the improved approximation \bar{u}_{i_1, i_2} is calculated in the following two steps.

1. The correction v_{i_1, i_2} is calculated by marching operator L_{st}^h with a right hand side being represented by the residual computed for the target operator L^h with the current approximation. The inflow boundary conditions for v are initialized with the zero values.

$$(1.6) \quad L_{st}^h v_{i_1, i_2} = f_{i_1, i_2} - L^h \tilde{u}_{i_1, i_2}; \quad v_{0, i_2} = 0.$$

2. The current approximation is corrected

$$(1.7) \quad \bar{u}_{i_1, i_2} = \tilde{u}_{i_1, i_2} + v_{i_1, i_2}.$$

The operator L_{st}^h is called the *driver* operator. The steps (1.6)-(1.7) can be repeated until the desired accuracy is reached.

In many papers (e.g., [5]), authors studying the defect-correction iteration for non-elliptic problems observed a slow convergence or even divergence in some common error norms for the initial iterations and good asymptotic convergence rates afterwards. This behavior is quite different from that demonstrated by the defect-correction method in solving elliptic problems where the asymptotic convergence rate is the slowest one. We realized that this “non-elliptic” feature is explained by some properties associated with the cross-characteristic interaction (e.g, dissipation) in the operators involved in the defect-correction iterations. Namely, this cross-characteristic interaction and the frequency of an incoming component define the *penetration distance* (also termed “survival distance” in [4]) of this component. The penetration distance is the distance from the inflow boundary on which the discrete solution of the homogeneous problem reasonably approximates the continuous one (i.e., the L_∞ norm of the relative discretization error is essentially less than 1). The ratio of penetration distances of the operators L^h and L_{st}^h determines the number of defect-correction sweeps required to get into the asymptotic convergence regime. Moreover, comparison of the penetration distances is a constructive and convenient tool allowing one to decide which grid is appropriate for a given problem, provided information is known regarding flow direction variations, the frequency content of inflow boundary conditions, the characteristic size of the domain, and the accuracy desired.

The analysis of the first differential approximations (FDA) (see [7]) to the operators involved in the defect-correction iterations is presented in Sec. 1.2. It provides us with some qualitative description of corresponding penetration distances. This analysis concludes that if the operators L^h and L_{st}^h have different approximation orders (the case described in Sec. 2) then the efficiency of defect-correction iterations is, actually, grid dependent. It means that the maximal number of sweeps which might be required to reach the asymptotic convergence rate (or to reduce the algebraic error to the truncation error level) on fine grids is larger than on coarse grids. This phenomenon relates to the fact that some *smooth* error components are poorly approximated by the driver operator. In other cases, when the operators L^h and L_{st}^h have the same approximation order (see Sec. 3), the defect-correction method can serve as a very efficient solver.

1.2. Poor Characteristic Component Approximation. The non-ellipticity of the operators to be analyzed introduces a new issue in the standard discretization analysis common for elliptic operators. The discretization error of a discrete elliptic operator regarding a given component is defined by (1) the operator’s approximation order and (2) frequencies of the component. For non-elliptic operators, the main factor is (3) the penetration distance d of this component. The penetration distance of an incoming component depends on its frequency ω , i.e., $d = d(\omega)$. Note, that in the homogeneous differential problem (1.1)-(1.3) all the incoming oscillations are translated along the characteristics without changing their phases and amplitudes. However, on a grid non-aligned with the characteristic, any discretization unavoidably introduces some numerical cross-characteristic interaction which damps amplitudes and/or shifts phases of

the incoming components. A quantitative measure of this numerical cross-characteristic interaction is the coefficient of the largest cross-characteristic derivative appearing in the first differential approximation to the operator under consideration. When the cross-characteristic interaction is strong, there are no approximation properties provided by the discrete operator beyond some $O(d)$ neighborhood of the inflow boundary. A discretization is considered to be accurate with respect to a given incoming component if and only if the penetration distance of this component is comparable with (or exceeds) the characteristic size of the domain. Of course, the penetration distance of a given component increases on grids with smaller mesh sizes. The coarsest grid on which the penetration distance approaches the characteristic size of the domain can be considered as the optimal grid for resolving this component. The expected discretization behavior (i.e, the discretization error of a p -th order accurate discrete operator is reduced by factor 2^p when the grid mesh size is refined to $h/2$) is observed only for grids which provide an accurate resolution for all the essential inflow components.

Let L^h be an accurate discretization with respect to some particular incoming component. To approximate the solution of L^h operator by solving some less accurate operator L_{st} (with a correspondingly shorter penetration distance), one has to iterate L_{st} as many times as needed to attain accuracy up to the L^h penetration distance. The following analysis shows that the required number of iterations depends on some power of N , where N is the number of grid points in the characteristic direction. To be precise, the number of iterations is proportional to $N^{\frac{p-r}{p+1}}$, where p and r are the approximation orders of operators L^h and L_{st} respectively. Below, we derive the predicted dependence for a particular case where $p = 2$ and $r = 1$.

Before proceeding with the analysis, let us introduce a definition. The components which are much more smooth in the characteristic direction than in other directions are referred to as the *characteristic components*.

The target operator L^h approximates the differential operator L from (1.1) with second order accuracy. It means that its first differential approximation (*FDA*) is

$$FDA(L^h) = \partial_\xi - C_2 h^2 \left(\partial_{\eta\eta\eta} + \partial_\xi B^2(\partial_\xi, \partial_\eta) \right),$$

where C_2 is a constant, $\eta = \frac{-tx+y}{\sqrt{1+t^2}}$ is the cross-characteristic coordinate and $B^2(\partial_\xi, \partial_\eta)$ is a linear combination of the second-order derivatives in ξ and η . For characteristic components (in terms of which $\partial_\eta \gg \partial_\xi$), this approximation is simplified to

$$(1.8) \quad FDA(L^h) \approx \partial_\xi - C_2 h^2 \partial_{\eta\eta\eta}.$$

Let the driver operator L_{st}^h have the first order accuracy. Then, its *FDA* taken for the characteristic components is

$$(1.9) \quad FDA(L_{st}^h) \approx \partial_\xi - C_1 h \partial_{\eta\eta},$$

where C_1 is a *positive* constant.

We are going to perform a half-space mode analysis for the first differential approximations to the operators L^h and L_{st}^h and demonstrate in this way that the driver operator L_{st}^h (and the whole defect-correction iterative process) is likely to approximate poorly some smooth characteristic components of the second order solution.

Following [2] and [4], the half-space mode analysis presented in this section is focused on approximating the characteristic components. It considers the discretizations of the homogeneous equation (1.1) on the half

space $\{(x, y) : x \geq 0\}$ with boundary conditions (on $x = 0$) being represented by one Fourier mode $e^{i\omega y}$ at a time. The purpose of this analysis is to estimate the penetration distance as a function of the incoming oscillations.

For the driver operator, we seek a bounded differentiable function $\phi(x, y)$ satisfying the following equation and boundary conditions

$$(1.10) \quad \partial_\xi \phi - C_1 h \partial_{\eta\eta} \phi = 0; \quad \phi(0, y) = e^{i\omega y}.$$

The exact solution can be written out as

$$\phi = e^{C_1 h \beta^2 \xi + \beta \eta},$$

where $\beta = a + ib$ is a complex number with a and b satisfying the system of the algebraic equations

$$\begin{cases} C_1 h (a^2 - b^2) t + a = 0; \\ 2C_1 h a b t + b = \sqrt{1 + t^2} \omega. \end{cases}$$

From the system, $a = O(h)$ and $b = \sqrt{1 + t^2} \omega + O(h)$. Therefore, the leading term of the bounded solution to (1.10) is

$$(1.11) \quad \phi \sim e^{-C_1 h (1+t^2) \omega^2 \xi + i \sqrt{1+t^2} \omega \eta}.$$

The factor $e^{\sqrt{1+t^2}(i\omega\eta)}$ describes the exact solution of the continuous problem while the factor $e^{-C_1 h (1+t^2) \omega^2 \xi}$ is the influence of the numerical cross-characteristic interaction. In the case of the first order driver, this is a dissipation which damps the amplitude. From (1.11), one can observe that the penetration distance on which this damping becomes $O(1)$ is proportional to $d^{(1)} = \frac{1}{\omega(\omega h)}$. In a similar way one can derive the penetration distance of a second order scheme, which is proportional to $d^{(2)} = \frac{1}{\omega(\omega h)^2}$. For even order schemes, the only difference is that the numerical cross-characteristic interaction usually affects the *phase* of the incoming component rather than the amplitude. The comparison of the penetration distances $d^{(1)}$ and $d^{(2)}$ implies that the number N_{sweeps} of defect-correction sweeps (1.6)-(1.7) needed to approximate the incoming component $e^{i\omega y}$ to the second order accuracy is

$$(1.12) \quad N_{sweeps} \sim \frac{d^{(2)}}{d^{(1)}} = \frac{1}{\omega h}.$$

It is obvious that this number increases when ω tends to zero. On the other hand, if ω is sufficiently small (e.g., the component is nearly constant) then the penetration distance for any scheme covers the entire domain and the desirable accuracy is achieved. This consideration implies that the worst case is the case $d^{(2)} \approx R$ and $d^{(1)} \ll R$, where R is a characteristic size of the domain ($R = \sqrt{1 + t^2}$ in our problem). Thus, on the given grid, the worst component is $\omega \sim R^{-\frac{1}{3}} h^{-\frac{2}{3}}$, and for this component

$$N_{sweeps} \sim \left(\frac{R}{h} \right)^{\frac{1}{3}}.$$

This meshsize dependence was first mentioned in [3]. It is really not very harmful and in many practical calculations it can hardly be noticed. However, an accurate choice of data in the numerical experiments allows us to observe this behavior.

Further, in Sec. 2, a defect-correction method with the first order driver is considered. We introduce another (nearly) precise *discrete* half-space mode analysis in Sec. 2.1 which then will be used to predict

the accuracy and the efficiency of the defect-correction iterations (tested in Sec. 2.3). Some analytical predictions about the asymptotic convergence rate of residual norms are made in Sec. 2.2 and are validated in Sec. 2.3. The comparison of the analytical and the numerical results for the defect-correction method with a second order driver is presented in Sec. 3. A very efficient adaptive multigrid algorithm yielding the approximate solution to a desired accuracy is proposed and tested in Sec. 4.

2. Defect-Correction Method with First Order Driver (DC1). The driver used in the DC1 algorithm is the first order upwind discretization of the convection operator (1.1).

$$(2.1) \quad \begin{aligned} L^1 u_{i_1, i_2} &= \frac{1}{\sqrt{1+t^2}h} \left((u_{i_1, i_2} - u_{i_1-1, i_2}) + t(u_{i_1, i_2} - u_{i_1, i_2-1}) \right); \\ i_1 &= 1, 2, \dots, N, \quad i_2 = 1, 2, \dots, N; \\ u_{0, i_2} &= g(i_2 h). \end{aligned}$$

This scheme is stable for downstream marching. In our case of y -directional periodicity, the marching of this scheme requires an implicit line-by-line rather than simple pointwise passage. The entire defect-correction iterative process has already been defined above in Sec. 1.1.

2.1. Half-Space Mode Analysis. In this section we exhibit a discrete half-space mode analysis of the defect-correction method which is distinct from the FDA analysis presented in Sec. 1.2: it considers the discretizations themselves rather than their differential approximation. This tool is much more accurate (and cumbersome at the same time). It can be used to explain in detail many phenomena observed in solving non-elliptic equations and provides a close prediction of the actual solution behavior.

This analysis considers each discretization on the half space as it is, while the boundary condition is represented by a Fourier component. In this way the original multidimensional problem is translated into a 1D discrete problem, where the frequencies of the boundary Fourier component are considered as parameters. To regularize the half-space problem, the solution is not allowed to grow faster than a polynomial function. The goal of this analysis is the comparison with each other of (1) the exact solution of the differential problem, (2) the exact solution of the discrete problem and (3) the approximate solutions at different stages of the solver.

2.1.1. Exact Solutions and Discretization Error. Choosing the domain to be $\{(x, y) : x \geq 0\}$, for each Fourier frequency ω_2 , the differential problem (1.2), (1.3) can be reformulated in the following way: find function $U(x, y)$ such that

$$\partial_x U = i\beta_\xi e^{i(\omega_1 x + \omega_2 y)}, \quad U(0, y) = e^{i\omega_2 y},$$

where $\beta_\xi = (\omega_1 + t\omega_2)/\sqrt{1+t^2}$ is the characteristic frequency ($\beta_\xi \approx 0$ for characteristic components). The exact solution of this problem is $U(x, y) = e^{i(\omega_1 x + \omega_2 y)}$.

The discrete counterpart is

$$(2.2) \quad L^h u_{i_1, i_2} = i\beta_\xi e^{i(\Omega_1 i_1 + \Omega_2 i_2)}, \quad u_{0, i_2} = e^{i\Omega_2 i_2}, u_{-1, i_2} = e^{i(-\Omega_1 + \Omega_2 i_2)},$$

where L^h is the target discrete operator, $\Omega_1 = \omega_1 h$ and $\Omega_2 = \omega_2 h$ are normalized frequencies.

We seek a solution of the discrete problem in the form

$$(2.3) \quad u_{i_1, i_2} = \phi_{i_1} e^{i\Omega_2 i_2}.$$

Then, the problem (2.2) can be reformulated for ϕ_{i_1} as

$$(2.4) \quad a_{-2}(\Omega_2)\phi_{i_1-2} + a_{-1}(\Omega_2)\phi_{i_1-1} + a_0(\Omega_2)\phi_{i_1} + a_1(\Omega_2)\phi_{i_1+1} = \sqrt{1+t^2}hi\beta_\xi e^{i\Omega_1 i_1};$$

$$(2.5) \quad \phi_0 = 1, \quad \phi_{-1} = e^{-i\Omega_1},$$

where

$$(2.6) \quad \begin{aligned} a_{-2}(\Omega_2) &= \frac{1}{4}; \\ a_{-1}(\Omega_2) &= -\frac{5}{4}; \\ a_0(\Omega_2) &= \frac{3}{4} + \frac{t}{4} \left(e^{-i2\Omega_2} - 5e^{-i\Omega_2} + 3 + e^{i\Omega_2} \right); \\ a_1(\Omega_2) &= \frac{1}{4}. \end{aligned}$$

The solution to (2.4), (2.5) is given by

$$(2.7) \quad \phi_{i_1} = W_0 e^{i\Omega_1 i_1} + (1 - W_0) (C_0 r_0^{i_1} + C_1 r_1^{i_1}),$$

where r_0 and r_1 are the roots of the cubic equation

$$a_{-2}(\Omega_2) + a_{-1}(\Omega_2)r + a_0(\Omega_2)r^2 + a_1(\Omega_2)r^3 = 0,$$

satisfying to $|r| \leq 1$,

$$\begin{aligned} W_0 &= \frac{\sqrt{1+t^2}hi\beta_\xi}{a_{-2}(\Omega_2)e^{-i2\Omega_2} + a_{-1}(\Omega_2)e^{-i\Omega_2} + a_0(\Omega_2) + a_1(\Omega_2)e^{i\Omega_2}}; \\ C_0 &= \frac{r_0(r_1 - e^{i\Omega_1})}{e^{i\Omega_1}(r_1 - r_0)}; \\ C_1 &= \frac{r_1(r_0 - e^{i\Omega_1})}{e^{i\Omega_1}(r_0 - r_1)}. \end{aligned}$$

We avoid here considering in details the exceptional cases where either the denominator in the expression for W_0 turns out to be zero or $r_0 = r_1$. In these cases, the form of the solution (2.7) remains the same while W_0 and/or $C_j (j = 0, 1)$ might turn to some linear functions of i_1 .

Thus, the discretization error is calculated as

$$\begin{aligned} U(i_1 h, i_2 h) - u_{i_1, i_2} &= \left[e^{i\Omega_1 i_1} - \phi_{i_1} \right] e^{i\Omega_2 i_2} \\ &= (1 - W_0) \left[e^{i\Omega_1 i_1} - C_0 r_0^{i_1} - C_1 r_1^{i_1} \right] e^{i\Omega_2 i_2}; \end{aligned}$$

2.1.2. DC1 Iteration. Let the boundary conditions be represented by a discrete Fourier mode $e^{i\Omega_2 i_2}$. Then, the first order driver operator can be rewritten as

$$L^1 \tilde{u}_{i_1, i_2} \equiv \frac{1}{h\sqrt{1+t^2}} \left[d_{-1}(\Omega_2) \tilde{\phi}_{i_1-1} + d_0(\Omega_2) \tilde{\phi}_{i_1} \right] e^{i\Omega_2 i_2},$$

where $\tilde{u}_{i_1, i_2} = \tilde{\phi}_{i_1} e^{i\Omega_2 i_2}$ is an approximate solution and

$$d_{-1}(\Omega_2) = -1; \quad d_0(\Omega_2) = 1 + t \left(1 - e^{-i\Omega_2} \right).$$

The general form of components appearing at any stage of the defect-correction iteration is

$$(2.8) \quad P(i_1) q^{i_1} e^{i\Omega_2 i_2},$$

where $P(i_1)$ is a complex-coefficient polynomial of i_1 and q ($|q| \leq 1$) is the base of the given component. This form is invariant under all the transformations occurring in the DC1 iteration. In fact, for any component, the only part to be changed is the polynomial $P(i_1)$ which will be referred to as the *amplitude* of the corresponding component $q^{i_1} e^{i\Omega_2 i_2}$. This allows us to analyze separately any building block of this algorithm, such as the calculation of residual or solving the driver equation. The underlying idea is to use computer capabilities already at the step of deriving an analytic representation for the current solution approximation. We actually analyze the response of each building block to an input component in the form (2.8). The output of the block is formulated in the same form (2.8), except that the block may produce several output components, differing in their bases q and/or frequencies Ω_2 .

Usually, the initial solution approximation satisfying the boundary conditions cannot be represented as a sum of a finite number of components in the form (2.8), e.g., the zero approximation inside with given (non-zero) boundary conditions at $i_1 = 0$ and $i_1 = -1$. In this case, the collection of analytical components (2.8) well describes the distant behavior of the approximation while an adjustment is still needed in the neighborhood of the boundary. The approximation in the neighborhood is given by an additional pointwise component

$$\begin{cases} B_{i_1} e^{i\Omega_2 i_2}, & 0 < i_1 \leq N_0 \\ 0 & \text{otherwise,} \end{cases}$$

where B_{i_1} is a complex-valued vector of the length N_0 . $N_0 = 0$ at the beginning for many reasonable initial approximations including (1) zero approximation, (2) solution of the driver equation, and (3) solution interpolated from the coarse grid in the framework of a 2-level multigrid solver. Then, N_0 is increased by 1 in each DC1 iteration. The segment $0 < i_1 \leq N_0$ we will call *the pointwise representation region* and the vector B will be called *the pointwise amplitude* while the domain $N_0 < i_1$ will be referred to as *the analytic representation region*.

Thus, the first necessary step in analyzing how the DC1 iteration affects the given approximation is to separate all the components (including the pointwise component) in the approximation.

Let $v_{i_1, i_2} = P(i_1) q^{i_1} e^{i\Omega_2 i_2}$ be a particular component of the current solution approximation. We are going to trace all the changes happening with the amplitude $P(i_1)$ of this component in a DC1 iteration. The changes in the pointwise component will be emphasized as well. An example of the DC1 iteration analysis will be presented below in this section.

Taking Residual.. The residual amplitude $R(i_1)$ of the component v_{i_1, i_2} is calculated as

$$R(i_1) = \Lambda - \frac{1}{h\sqrt{1+t^2}} \left[a_{-2}(\Omega_2)q^{-2}P(i_1-2) + a_{-1}(\Omega_2)q^{-1}P(i_1-1) + a_0(\Omega_2)P(i_1) + a_1(\Omega_2)qP(i_1+1) \right],$$

where $\Lambda = i\beta_\xi$ if $q^{i_1}e^{i\Omega_2 i_2}$ is the right-hand side component ($q = e^{i\Omega_1}$), otherwise $\Lambda = 0$.

Let $N'_0 = N_0 + 2$ and $B_{i_1} = 0, i_1 > N_0$. Then, the pointwise residual function is computed in the following way

$$R_{i_1}^{\text{pt}} = -\frac{1}{h\sqrt{1+t^2}} \begin{cases} a_{-2}(\Omega_2)S_{-1} + a_{-1}(\Omega_2)S_0 + a_0(\Omega_2)B_{i_1} + a_1(\Omega_2)B_{i_1+1}, & i_1 = 1; \\ a_{-2}(\Omega_2)S_0 + a_{-1}(\Omega_2)B_{i_1-1} + a_0(\Omega_2)B_{i_1} + a_1(\Omega_2)B_{i_1+1}, & i_1 = 2; \\ a_{-2}(\Omega_2)B_{i_1-2} + a_{-1}(\Omega_2)B_{i_1-1} + a_0(\Omega_2)B_{i_1} + a_1(\Omega_2)B_{i_1+1}, & 3 \leq i_1 \leq N'_0; \\ 0, & \text{otherwise.} \end{cases}$$

where S_{-1} and S_0 are the boundary conditions (at $i_1 = -1$ and $i_1 = 0$ respectively) in the problem associated with the pointwise representation region.

Correction Calculation.. The amplitude $C(i_1)$ of the correction to the component v_{i_1, i_2} is calculated from the equation

$$d_{-1}(\Omega_2)q^{-1}C(i_1-1) + d_0(\Omega_2)C(i_1) = h\sqrt{1+t^2}R(i_1).$$

If v_{i_1, i_2} is not an eigencomponent for the driver operator ($q \neq d_1 = -d_0(\Omega_2)/d_{-1}(\Omega_2)$), then the power of the polynomial $C(i_1)$ is the same as of the polynomial $R(i_1)$; otherwise the $C(i_1)$ power is higher.

To satisfy the zero conditions at the incoming boundary $i_1 = 0$ which accompany the correction equation, one has to complete the correction with the eigencomponent $D_0 d_1^{i_1} e^{i\Omega_2 i_2}$ with the amplitude

$$D_0 = -C(0).$$

The pointwise correction $C_{i_1}^{\text{pt}}$ is calculated from the following system of linear equations.

$$\begin{cases} C_{N'_0}^{\text{pt}} = 0 \\ d_{-1}(\Omega_2)C_{i_1}^{\text{pt}} + d_0(\Omega_2)C_{i_1+1}^{\text{pt}} = h\sqrt{1+t^2}R_{i_1+1}^{\text{pt}}, 0 < i_1 < N'_0. \end{cases}$$

The amplitude D_1 of the accompanying eigencomponent is computed by

$$D_1 = -\frac{h\sqrt{1+t^2}R_1^{\text{pt}} - d_0(\Omega_2)C_1^{\text{pt}}}{d_{-1}(\Omega_2)}.$$

New Amplitude.. The new amplitude $\tilde{P}(i_1)$ of the component v_{i_1, i_2} is calculated as

$$\tilde{P}(i_1) = P(i_1) + C(i_1).$$

The corrected pointwise amplitude \tilde{B}_{i_1} and the new boundary \tilde{N}_0 of the pointwise representation region are

$$\tilde{B}_{i_1} = B_{i_1} + C_{i_1}^{\text{pt}}; \quad \tilde{N}_0 = N_0 + 1.$$

The amplitude $D(i_1)$ of the eigencomponent is also changed to $\tilde{D}(i_1)$

$$\tilde{D}(i_1) = D(i_1) + D_0 + D_1.$$

2.1.3. Discretization of Outflow Boundary Conditions. The discretization of the outflow boundary conditions can be taken into account as well. Discretized outflow boundary conditions usually imply some special discretization stencil different from that in the interior. In order to incorporate this feature into the analysis we have to introduce another pointwise representation zone near the outflow boundary. In other words, an additional pointwise component is required to make the half-space analysis be precise for all the y -periodic problems. In the analysis tests below (Sec. 2.3.1) we did not implement this adjustments. It was realized that the analysis is actually precise even without this special care about the outflow boundary conditions.

2.1.4. Example of Analysis. Let us consider the homogeneous problem ($\beta_\xi = 0$) with boundary conditions given by (2.5) and the zero initial approximation inside of the half-space $0 < i_1$. At the beginning the only component involved in calculation is the zero-length ($N_0 = 0$) pointwise component. The problem associated with this component is

$$\begin{aligned} a_{-2}(\Omega_2)B_{i_1-2} + a_{-1}(\Omega_2)B_{i_1-1} + a_0(\Omega_2)B_{i_1} + a_1(\Omega_2)B_{i_1+1} &= 0; \\ S_0 &= 1, \quad S_{-1} = e^{-i\Omega_1} \end{aligned}$$

1. The extended boundary of the pointwise approximation region is $N'_0 = 2$.
2. The residual function is

$$\begin{cases} R_1^{\text{pt}} = -\frac{1}{h\sqrt{1+t^2}} \left(a_{-2}(\Omega_2)S_{-1} + a_{-1}(\Omega_2)S_0 \right); \\ R_2^{\text{pt}} = -\frac{1}{h\sqrt{1+t^2}} a_{-2}(\Omega_2)S_0; \\ R_{i_1}^{\text{pt}} = 0, 2 < i_1. \end{cases}$$

3. A non-zero correction proves to be only at point $i_1 = 1$

$$\begin{aligned} C_1^{\text{pt}} &= \frac{h\sqrt{1+t^2}R_2^{\text{pt}}}{d_{-1}(\Omega_2)}; \\ B_1 &= C_1^{\text{pt}}; \\ N_0 &= 1; \end{aligned}$$

The eigenvector is introduced with the amplitude

$$D_1 = -\frac{h\sqrt{1+t^2}R_1^{\text{pt}} - d_0(\Omega_2)C_1^{\text{pt}}}{d_{-1}(\Omega_2)}.$$

4. The approximation obtained at the end of the first DC1 iteration is

$$\begin{aligned} \tilde{u}_{i_1, i_2} &= Q(i_1)e^{i\Omega_2 i_2} \\ Q(i_1) &= \begin{cases} D_1 d_1 + B_1, & i_1 = 1; \\ D_1 d_1^i, & i_1 > 1; \end{cases} \end{aligned}$$

5. On the next iteration the initial approximation contains the eigenvector with the amplitude $D(i_1) = D_1$. Therefore, the boundary conditions in the problem associated with the pointwise component is changed to

$$S_0 = 1 - D(0), \quad S_{-1} = e^{-i\Omega_1} - D(-1)/d_1.$$

The calculations can be continued. Approximations obtained in these iterations can always be represented as

$$\begin{aligned}\tilde{u}_{i_1, i_2} &= Q(i_1)e^{i\Omega_2 i_2}, \\ Q(i_1) &= \begin{cases} D(i_1)d_1^{i_1} + B_{i_1}, & 1 \leq i_1 \leq N_0; \\ D(i_1)d_1^{i_1}, & N_0 < i_1; \end{cases}\end{aligned}$$

2.1.5. Algebraic and Total Errors. Let additional component $w_{i_1, i_2} = W(i_1)e^{i\Omega_1 i_1}e^{i\Omega_2 i_2}$ be involved into the calculation due to the right-hand side function; then, after any iteration the current approximation representation is a sum of this component, the eigenvector $d_{i_1, i_2} = D(i_1)d_1^{i_1}e^{i\Omega_2 i_2}$, and the pointwise component. Thus, the current solution approximation is

$$(2.9) \quad \begin{aligned}\tilde{u}_{i_1, i_2} &= Q(i_1)e^{i\Omega_2 i_2}, \\ Q(i_1) &= \begin{cases} W(i_1)e^{i\Omega_1 i_1} + D(i_1)d_1^{i_1} + B_{i_1}, & 1 \leq i_1 \leq N_0; \\ W(i_1)e^{i\Omega_1 i_1} + D(i_1)d_1^{i_1}, & N_0 < i_1. \end{cases}\end{aligned}$$

The *algebraic error* function which is the difference between the exact and approximate solutions of the discrete problem is given by

$$(2.10) \quad \tilde{u}_{i_1, i_2} - u_{i_1, i_2} = \left[Q(i_1) - \left(W_0 e^{i\Omega_1 i_1} + C_0 r_0^{i_1} + C_1 r_1^{i_1} \right) \right] e^{i\Omega_2 i_2}.$$

The *total error* function defined as the difference between an approximate solution of the discrete problem and the exact solution of the differential problem is calculated as

$$(2.11) \quad \tilde{u}_{i_1, i_2} - U(i_1 h, i_2 h) = \left[Q(i_1) - e^{i\Omega_1 i_1} \right] e^{i\Omega_2 i_2}.$$

Involving other components, either due to a non-zero initial approximation or since the algorithm itself produces additional components, extends the number of items in (2.9) with straightforward changes in the algebraic and total error expressions (2.10) and (2.11).

2.2. Convergence in Residual Norms. The matrix analysis described in this section can be considered as the asymptotic case of the half-space analysis (with the discretized outflow boundary conditions) exhibited in Sec. 2.1. In this asymptotic regime, the pointwise representation region covers all the domain. Let the problem (1.1)-(1.3) be defined on a layer $(x, y) \in [0, 1] \times (-\infty, +\infty)$ with the input data (functions $F(x, y)$ and $g(x, y)$) such that the function $U(x, y) = \Phi(x)e^{i\omega y}$ is the exact solution of the problem. The approximate solution of the corresponding discrete problem (1.4) is sought in the form (2.3). The problem for the discrete function ϕ_{i_1} is derived similar to the problem (2.4)-(2.5)

$$(2.12) \quad \begin{aligned}\phi_0 &= \Phi(0), & \phi_{-1} &= \Phi(-h), \\ a_{-2}(\Omega_2)\phi_{i_1-2} + a_{-1}(\Omega_2)\phi_{i_1-1} + a_0(\Omega_2)\phi_{i_1} + a_1(\Omega_2)\phi_{i_1+1} \\ &= h\sqrt{1+t^2}\left(\Phi_x(i_1 h) + it\omega\Phi(i_1 h)\right), & i_1 &= 1, \dots, N-1; \\ b_{-2}(\Omega_2)\phi_{N-2} + b_{-1}(\Omega_2)\phi_{N-1} + b_0(\Omega_2)\phi_N &= h\sqrt{1+t^2}\left(\Phi_x(1) + it\omega\Phi(1)\right).\end{aligned}$$

Functions a_j ($j = -2, -1, 0, 1$) are defined in (2.6),

$$b_{-2}(\Omega_2) = \frac{1}{2};$$

$$(2.13) \quad \begin{aligned} b_{-1}(\Omega_2) &= -2; \\ b_0(\Omega_2) &= \frac{3}{2} + \frac{t}{2} \left(e^{-i2\Omega_2} - 4e^{-i\Omega_2} + 3 \right). \end{aligned}$$

Let the N -dimensional vector $\tilde{\phi} = (\tilde{\phi}_{i_1})$, $(i_1 = 1, \dots, N)$ be an approximate solution to (2.12) with the algebraic error $\bar{e} = (e_{i_1})$, i.e.,

$$\tilde{\phi} = \bar{\phi} - e_{i_1},$$

where $\bar{\phi}$ is the exact solution to (2.12).

The correction $\bar{\delta} = (\delta_{i_1})$ is calculated from the linear system of N equations

$$D\bar{\delta} = -T\bar{e},$$

where N -by- N banded matrices T and D correspond to the target operator and to the driver operator respectively.

$$T = \begin{pmatrix} a_0 & a_1 & 0 & 0 & 0 & \cdots & 0 & 0 & 0 & 0 \\ a_{-1} & a_0 & a_1 & 0 & 0 & \cdots & 0 & 0 & 0 & 0 \\ a_{-2} & a_{-1} & a_0 & a_1 & 0 & \cdots & 0 & 0 & 0 & 0 \\ 0 & a_{-2} & a_{-1} & a_0 & a_1 & \cdots & 0 & 0 & 0 & 0 \\ \vdots & \vdots \\ 0 & 0 & 0 & 0 & 0 & \cdots & a_{-2} & a_{-1} & a_0 & a_1 \\ 0 & 0 & 0 & 0 & 0 & \cdots & 0 & b_{-2} & b_{-1} & b_0 \end{pmatrix},$$

$$D = \begin{pmatrix} d_0 & 0 & 0 & \cdots & 0 & 0 \\ d_{-1} & d_0 & 0 & \cdots & 0 & 0 \\ 0 & d_{-1} & d_0 & \cdots & 0 & 0 \\ \vdots & \vdots & \vdots & \vdots & \vdots & \vdots \\ 0 & 0 & 0 & \cdots & d_{-1} & d_0 \end{pmatrix}.$$

Then, the amplification matrix G_e of the defect correction iteration

$$\bar{e}^{\text{new}} = G_e \bar{e}$$

becomes

$$G_e = I - D^{-1}T.$$

Since the residual is usually used in practice to monitor the error, we can modify G_e to measure the residual reduction, as

$$G_r = TG_eT^{-1}$$

so that

$$\bar{r}^{\text{new}} = G_r \bar{r}$$

where

$$\bar{r} = -T\bar{e}$$

represents the discrete residual. If we wish to bound the amplification of the residual, we could use the spectral radius of G_r ($\rho(G_r)$) or the L_2 -norm of the matrix G_r ($\|G_r\|_2 = \sqrt{\rho(G_r^*G_r)}$). The spectral radius $\rho(G_r)$ is usually referred to as the asymptotic convergence rate, i.e., the rate corresponding to a large number of iterations. The L_2 -norm ($\|G_r\|_2$) indicates the “worst” possible convergence rate.

2.3. Numerical Tests.

2.3.1. Verification of Analytical Predictions: Discretization Accuracy Test. The discretization accuracy of an operator on the grid of meshsize h for a *characteristic* component $e^{i(\omega_1 x + \omega_2 y)}$ (where $\omega_1 + t\omega_2 \approx 0$) is defined by the penetration distance of this component. (Sec Sec. 1.2.) The first differential approximation to the target second order accurate discrete operator (1.4) is defined by

$$FDA(L^h) = \partial_x + t\partial_y - \frac{h^2}{12\sqrt{1+t^2}} \left(\partial_{xxx} + t\partial_{yyy} \right).$$

For characteristic components, it turns to

$$(2.14) \quad FDA(L^h) = \partial_\xi - \frac{h^2}{12(1+t^2)^2} (-t^3 + t) \partial_{\eta\eta\eta},$$

where the non-alignment parameter t and the characteristic variables ξ and η are defined in Sec. 1. Notice, when $t \approx 1$, the coefficient of the third derivative with respect to η vanishes in the FDA and the next term (the fourth derivative) becomes important.

In the general case $0 \leq t \leq 1$, the discretization error of L^h ($DE(L^h)$) can be approximately calculated from the asymptotic solution of the half-space problem associated with (2.14). The derived estimate is

$$DE(L^h) = e^{i(\omega_1 x + \omega_2 y)} \left(1 - e^{-\frac{\xi}{d_2}} \right),$$

where

$$(2.15) \quad d_2 = \frac{-i12\sqrt{1+t^2}}{\omega_2(\omega_2 h)^2(-t^3+t)}.$$

DEFINITION 1. We say that a discretization has the accuracy ϵ for the given characteristic component with the inflow y -directional frequency ω_2 on the distance δ (measured along the characteristic) from the boundary if the following inequality holds

$$(2.16) \quad \left| 1 - e^{-\frac{\xi}{d}} \right| \leq \epsilon, \quad \text{for } \xi \leq \delta,$$

where d is the normalized penetration distance of the given characteristic component. Note, that ϵ defines the *relative* accuracy, hence $0 \leq \epsilon \leq 1$ and $\epsilon \approx 1$ indicates very poor accuracy. For operator (1.4), $d = d_2$ and the penetration distance of the ϵ -accuracy is estimated from (2.16) as

$$(2.17) \quad \delta_2 = |d_2| \arccos(1 - \epsilon^2/2).$$

TABLE 2.1
Penetration distances (in meshsizes) of the 1% accuracy.

t	ω_2	Penetration distances					
		target operator			driver operator		
		$\delta_a^{(2)}$	$\delta_A^{(2)}$	$\delta_N^{(2)}$	$\delta_a^{(1)}$	$\delta_A^{(1)}$	$\delta_N^{(1)}$
0.2	2π	256	256	256	139.034	139	139
	4π	256	256	256	34.758	34	34
	8π	256	256	256	8.69	8	8
	10π	256	256	256	5.561	5	5
	16π	82.564	81	81	2.172	2	2
0.6	2π	256	256	256	34.758	34	34
	4π	256	256	256	8.69	8	8
	8π	256	256	256	2.172	2	2
	10π	169.092	162	162	1.39	1	1
	16π	41.282	37	37	0.543	0	0
0.8	2π	256	256	256	23.172	23	23
	4π	256	256	256	5.793	5	5
	8π	256	256	256	1.448	1	1
	10π	225.456	181	181	0.927	0	0
	16π	55.043	35	35	0.362	0	0

The first differential approximation to the first order accurate driver operator (2.1) taken for the characteristic components is given by

$$\begin{aligned}
 FDA(L^1) &= \partial_\xi - \frac{h}{2(1+t^2)^{\frac{3}{2}}} (t^2+t) \partial_{\eta\eta}, \\
 d_1 &= \frac{2\sqrt{1+t^2}}{\omega_2(\omega_2 h)(t^2+t)}
 \end{aligned}
 \tag{2.18}$$

and the ϵ -accuracy penetration distance is

$$\delta_1 = -d_1 \ln(1 - \epsilon).
 \tag{2.19}$$

The first test we perform to validate the discrete half-space analysis from Sec. 2.1 and analytical expressions (2.17) and (2.19) for penetration distances of characteristic components. We calculate penetration distances of $\epsilon = 0.01$ accuracy for different values of t and ω_2 for operators (1.4) and (2.1). Our aim is to compare the following distances from the boundary (measured in meshsizes) : (1) calculated by formulas (2.17) and (2.19) ($\delta_a^{(j)} = \delta_j/\sqrt{1+t^2}/h$, $j = 1, 2$), (2) derived from the half-space analyses from Sec. 2.1 ($\delta_A^{(j)}$) and (3) computed in direct numerical simulations ($\delta_N^{(j)}$). In analytical calculations, the exact solution of the differential problem (1.1), (1.3) is always assumed to be $e^{i\omega_2(-tx+y)}$. In direct numerical simulations the exact solution has been chosen to be $\sin(\omega_2(-tx+y))$. The numerical distance is considered to be m if the L_∞ norm of the discretization error on $(m+1)$ -th vertical line is greater than 0.01. The simulation grid is 257×257 . If in analytical calculations the result exceeded 256 (the penetration distance covers all the domain) it has been set to 256. Table 2.1 contains the test results. The two obvious conclusions are

1. The discrete half-space analysis is actually precise. In all the tests, the results predicted by this analysis and obtained in real numerical calculations coincide.
2. The inequality (2.16) provides a good estimate of the penetration distance, especially, for the first order operator or for small angles of attack ($t \leq 0.6$). Some deterioration in predicting the second order operator penetration distances for nearly diagonal alignment is explained by the fact that the penetration distance in case of 45° angle of attack ($t = 1$) is determined by the *third order term* which is not taken into account in calculating d_2 . Nevertheless, the estimate obtained from (2.16) seems to be reliable to predicting the key property: whether the penetration distance is comparable with (or larger than) the characteristic size of the domain. Moreover, it gives us a possibility to estimate the ratio between the penetration distances of the target and driver operators even on very coarse grids where one of the distances (or both of them) is shorter than one mesh size.

2.3.2. Convergence to Within the Given Accuracy. Let function $U(x, y) = e^{i(\omega_1 x + \omega_2 y)}$ be the exact solution of (1.1) and (1.3). We can reformulate the discrete problem in the following way: we are looking for a discrete function \tilde{u}_{i_1, i_2} (an approximate solution to (1.4)) that possesses the *total error* (in the L_∞ norm) which is not greater than given ϵ , i.e.,

$$\max_{i_1, i_2} \left| \tilde{u}_{i_1, i_2} - U(i_1 h, i_2 h) \right| \leq \epsilon.$$

In order to find such a solution, the discretization error of the target operator, of course, should satisfy

$$(2.20) \quad \max_{i_1, i_2} \left| \bar{u}_{i_1, i_2} - U(i_1 h, i_2 h) \right| \leq \epsilon,$$

where \bar{u}_{i_1, i_2} is the exact solution of (1.4). This, in particular, implies that the target operator penetration distance δ_2 of the ϵ -accuracy on the uniform grid with spacing h for incoming frequency ω_2 is larger than the characteristic size R of the domain ($R = \sqrt{1 + t^2}$ in our case). The condition (2.20) actually defines the coarsest possible grid on which the desired ϵ -accuracy can be achieved. The goal of converging within the discretization error, which is typical in FMG type algorithms, can be considered as a particular case where ϵ is the target operator discretization error.

The analysis from Sec. 2.1 provides us with an upper bound $\bar{\omega}$ for frequencies of incoming Fourier modes ω_2 satisfying (2.20). The same analysis predicts the number of defect-correction sweeps N_{sweeps} required to achieve an approximation possessing the ϵ -accuracy. Both $\bar{\omega}$ and N_{sweeps} depend, of course, on the mesh size h of the given grid, on the desired accuracy ϵ , and on the non-alignment parameter t .

Fig. 1 demonstrates the typical behavior of $\bar{\omega}$ and N_{sweeps} as functions of the mesh size h . In all the experiments we performed, the 1%-accuracy ($\epsilon = 0.01$) was picked on. The choice of angles of attack was representative. For simplicity, we always started from the initial approximation in the interior of the domain ($i_1 > 0$) obtained from the solution of the driver operator.

The results corroborate the conclusions made in Sec. 1.2 about the growth of the number of cycles required to achieve an approximation possessing the ϵ -accuracy. For obviousness we added to the lower plot on Fig. 2.1 the solid line corresponding to the function $h^{-1/3}$.

The practical conclusions are the following.

1. The number of DC1 iterations required to achieve a given accuracy grows as some (negative) power of h (approximately $h^{-\frac{1}{3}}$).
2. For any given (continuous) boundary conditions, the analysis is able to provide predictions of the grid required to solve this problem to a desired accuracy and how many defect-correction sweeps should be performed to achieve this accuracy.

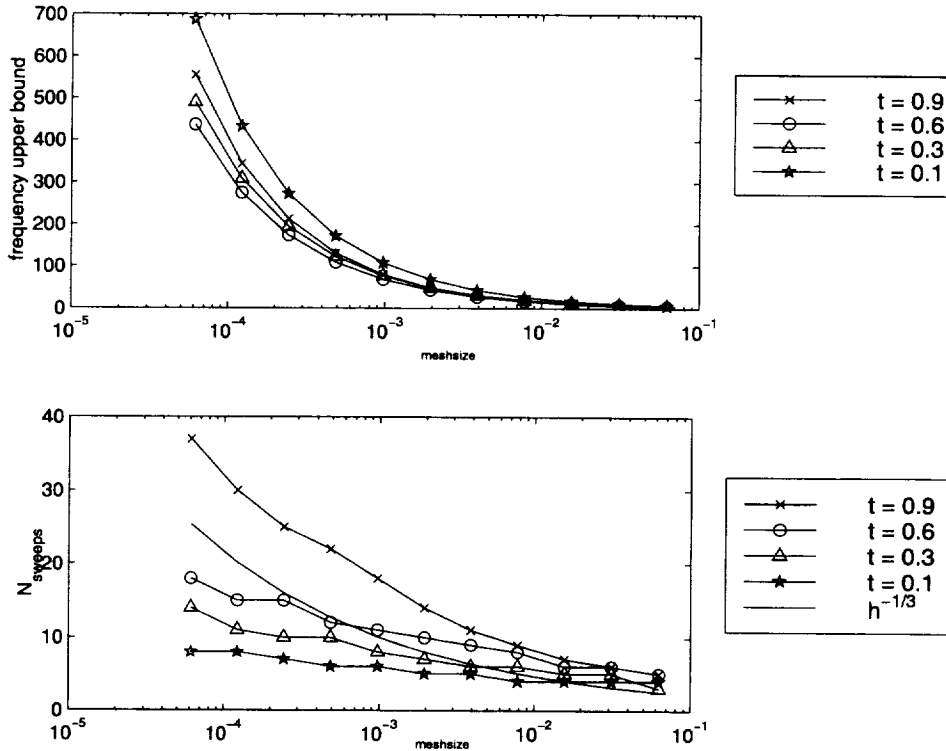


FIG. 2.1. $\bar{\omega}$ and N_{sweeps} as functions of the meshsize h .

3. If the flow direction is variable, one should select $\bar{\omega}$ and N_{sweeps} such that $\bar{\omega}$ satisfies (2.20) for all the possible angles of attack and N_{sweeps} iterations provide the desired accuracy for characteristic components with the incoming frequency $\bar{\omega}$ for any possible t .
4. A smart choice of the initial approximation (e.g., the initial approximation being interpolated from the coarse grid in the framework of an FMG solver) can sometimes reduce N_{sweeps} but the qualitative behavior remains the same: the number of required defect-correction iterations grows as some negative power of h in passing to finer grids.

There are several ways to change the algorithm in order to get N_{sweeps} independent on the meshsize h :

1. The first possibility which is studied in Sec. 3 is to apply a driver of the same approximation order as the target operator. This cure is actual only for second order operators since for higher-order scheme there are no stable upwind discretizations.
2. The second way is to use a predictor-corrector technique for solving the target operator. This method suggests some marching along the flow direction. If this is possible (there are no recirculation zones), then this approach is, probably, one of the best allowing to achieve an optimal efficiency.
3. The third method is a smart multigrid algorithm which employs the coarse-grid operators approximating the *characteristic component FDA* of the target operator.

The two latest approaches are the subjects of future papers.

Before going to the defect-correction scheme with the second order driver we consider the asymptotic convergence of the first order driver scheme.

2.3.3. Asymptotic Convergence. First of all we believe that the most important characteristic of the solver efficiency is the ability to fast solve the problem to the desired accuracy. The fact that the accuracy

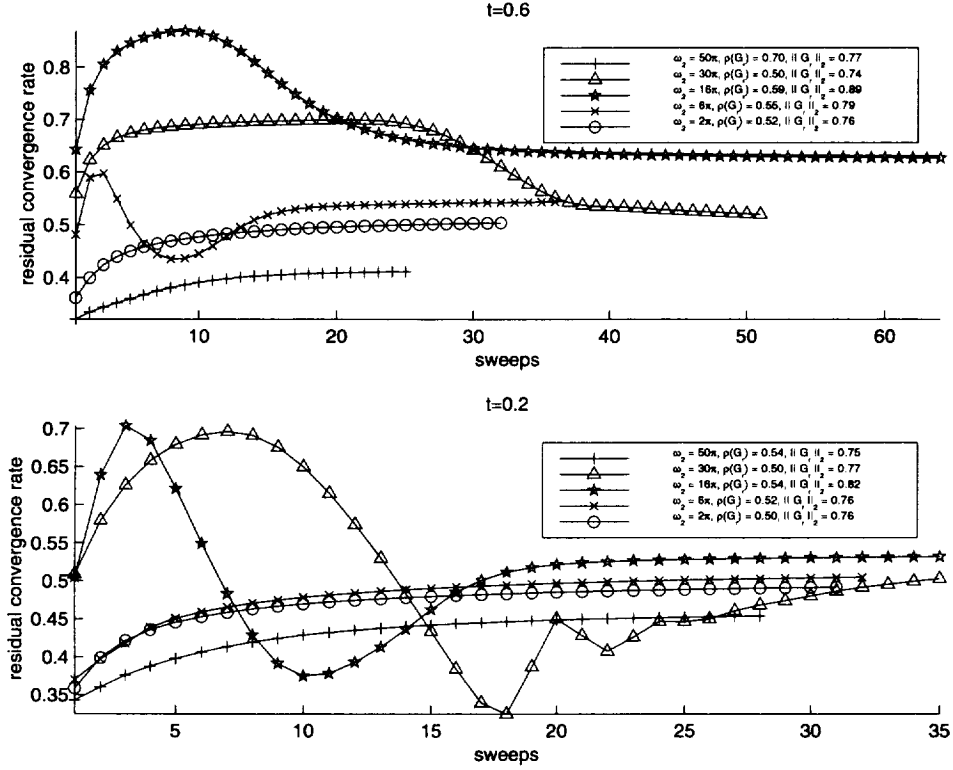


FIG. 2.2. DC1: residual convergence rate history.

has already been reached can be established from the comparison of the solutions on grids with different meshsizes. In this view, delivering the residuals to the computer zero is less important. Other criteria (rather than the vanished residuals) should be used to decide on stopping iterations on the given grid and passing to a finer grid. However, the principal possibility to drive residuals to the computer zero is considered to be useful. Tests below demonstrate that DC1 iterations possess this property.

It was observed by many researchers that the asymptotic convergence rate of the defect-correction solver for (1.4) is about 0.5 per iteration. (In [5], authors emphasized that the asymptotic convergence rate can somehow deteriorate for the central and the pure upwind target discretizations.) This asymptotic convergence rate can actually be further improved by a proper residual weighting ([1] suggests the weight 2/3 for the pure upwind operator). However, we already mentioned that this good convergence rate is only achieved after many sweeps with a much poorer convergence. Fig. 2.2 demonstrate the residual convergence history for different representative vales of the incoming frequency ω_2 and the non-alignment parameter t . In the legend, the corresponding amplification factors (the asymptotic convergence rate ($\rho(G_r)$) and the convergence rate bound ($\|G_r\|_2$) calculated by the methodology explained in Sec. 2.2 are shown. In all the numerical tests performed for the homogeneous problem (1.4) ($f_{i_1, i_2} = 0$) on the uniform grid with meshsize $h = 2^{-6}$, the iterations was stopped when the residual L_2 norm became less than 10^{-10} . The results of the tests can be summarized as following.

1. The asymptotic convergence rate is always good enough and the $\rho(G_r)$ estimate is its accurate prediction. However, this good convergence is manifested only either on very fine grids or after a lot of iterations.
2. The bound $\|G_r\|_2$ is not very sharp in the presented tests. The full space Fourier analysis (eliminating

the characteristic components from the consideration) gives a similar estimate (see [5]). It, probably, means that in order to observe this “worst” behavior one should test non-homogeneous problems.

3. The number of sweeps required to get into the asymptotic convergence regime is roughly proportional to the ratio $\min(R, d_2)/d_1$, where d_1 (2.18) and d_2 (2.15) are the first and the second order penetration distance parameters respectively. This number grows roughly as $h^{-1/3}$ in passing to finer grids.
4. For any given incoming frequency ω_2 , there is a grid with small enough meshsize h ($d_1 = O(R)$) on which the defect-correction iterations demonstrate the asymptotic convergence rate from the very beginning.

3. Defect-Correction Method with Second Order Driver (DC2). The second order accurate upwind discretization is defined as

$$(3.1) \quad L_n^2 u_{i_1, i_2} = \frac{1}{2\sqrt{1+t^2}h} \left(\left(3u_{i_1, i_2} - 4u_{i_1-1, i_2} + u_{i_1-2, i_2} \right) \right. \\ \left. + t \left(3u_{i_1, i_2} - 4u_{i_1, i_2-1} + u_{i_1, i_2-2} \right) \right); \\ i_1 = 1, 2, \dots, N, \quad i_2 = 1, 2, \dots, N; \\ u_{0, i_2} = g(i_2 h), \quad u_{-1, i_2} = g'(i_2 h).$$

It is stable in marching and can serve as a driver for the defect-correction iterations.

We tested the DC2 iterations for the same test-cases as in Sec. 2. In all the experiments on all the grids, the number of DC2 iterations required to get 1% accuracy did not exceed 3 (including the first sweep marching the driver operator (3.1) to obtain the initial approximation). The residual convergence rate history shown on Fig. 3.1 confirms the predicted efficiency of the defect-correction method with the second order driver and demonstrates the reliability of the residual convergence analysis introduced in Sec. 2.2.

4. Adaptive Multigrid Algorithm (AMA). Any adaptive multigrid solver is usually required to make two important decisions. The first is to decide on stopping iterating on the given grid and proceeding to the next fine grid. The second issue is to realize that the required approximation is achieved and finish its work.

Some prior information being incorporated into the solver can improve its performance a lot. For example, if the amplitudes of all the significant (for the given ϵ -accuracy) Fourier components of the inflow boundary conditions can be estimated, then many calculations can be performed in advance. In particular, using the half-space analysis for the highest frequency essential Fourier component, one can find the optimal grid spacing h and the number of the defect-correction iterations on that grid required to achieve the desired accuracy. Then, a single-grid algorithm performing the necessary N_{sweeps} iterations seems to be the optimal solver.

For general boundary conditions, this approach does not work. In case of general boundary conditions, however, all the decision should be done “automatically” employing only the data computed during the solution process. The algorithm we propose in this section is based on the full multigrid methodology where the comparison between solutions on different grids becomes a criterion for stopping further refinement. The adaptive multigrid algorithm solving the problem to the ϵ -accuracy can be recursively defined in the following 5 steps:

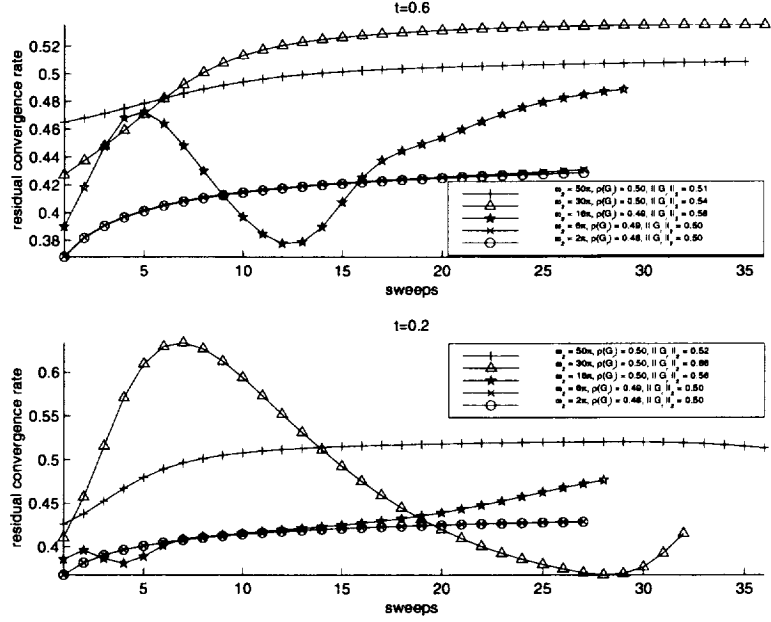


FIG. 3.1. DC2: residual convergence rate history.

1. Let u^{2h} be the solution on the grid with meshsize $2h$. On the grid with meshsize h for the given ϵ -accuracy, the highest possible incoming frequency $\bar{\omega}$ for which this accuracy is achievable is calculated from the half-space analysis. The required number of the sweeps N_{sweeps} is defined as well.
2. The initial approximation on the interior of the h -grid is obtained by (bilinear) solution interpolation from the $2h$ -grid.
3. One defect-correction iteration is performed and an approximate solution \tilde{u}^h is obtained.
4. If the L_∞ norm of the difference between \tilde{u}^h and u^{2h} is less than ϵ then \tilde{u}^h is the final solution. Solver finishes its work.

Otherwise, additional defect-correction sweeps are performed. The iterations on the h -grid are stopped when either the L_∞ norm of the difference between the two successive approximations becomes less than ϵ or the total number of sweeps (including the first one performed in the Step 3) reaches the corresponding h -grid N_{sweeps} . In fact, as one can see from the numerical tests below, the latter tolerance was reached only on relatively coarse grids, where the target discretization has no accuracy at all. The last approximation is considered as the h -grid solution u^h .

5. h replaced with $h/2$. Go to Step 1 for the next fine grid.

Table 4 collects $\bar{\omega}$ and N_{sweeps} values on grids with different meshsizes h for $\epsilon = 0.01$. In this table, $\bar{\omega}$ is the highest frequency resolved in the target second order operator on the h -grid to the ϵ -accuracy for *any angle of attack* ($0 \leq t \leq 1$) and N_{sweeps} is the number of DC1 sweeps ensures the convergence within this accuracy. We found from the analysis and checked in numerical tests that on grids with $h \geq 2^{-7}$ the maximal cross-characteristic interaction defining $\bar{\omega}$ is observed for the diagonal alignment case ($t = 1$) while on the finer grids the strongest interaction occurs at $t \approx 0.6$. The maximal N_{sweeps} is always found at the diagonal alignment.

If the driver is second order accurate then on all the grids the number of required DC2 sweeps is bounded to $N_{\text{sweeps}} = 3$.

The Figs. 4.1 and 4.2 demonstrate the performance of AMA based on DC1 and DC2 defect-correction

TABLE 4.1
Limits for iterating DC1 scheme on different grids.

h	2^{-4}	2^{-5}	2^{-6}	2^{-7}	2^{-8}	2^{-9}	2^{-10}	2^{-11}	2^{-12}	2^{-13}	2^{-14}
$\bar{\omega}$	1.1π	1.9π	3.2π	5.4π	8.6π	13.7π	21.8π	34.7π	55.1π	87.6π	139.1π
N_{sweeps}	5	6	7	9	9	10	12	14	16	18	21

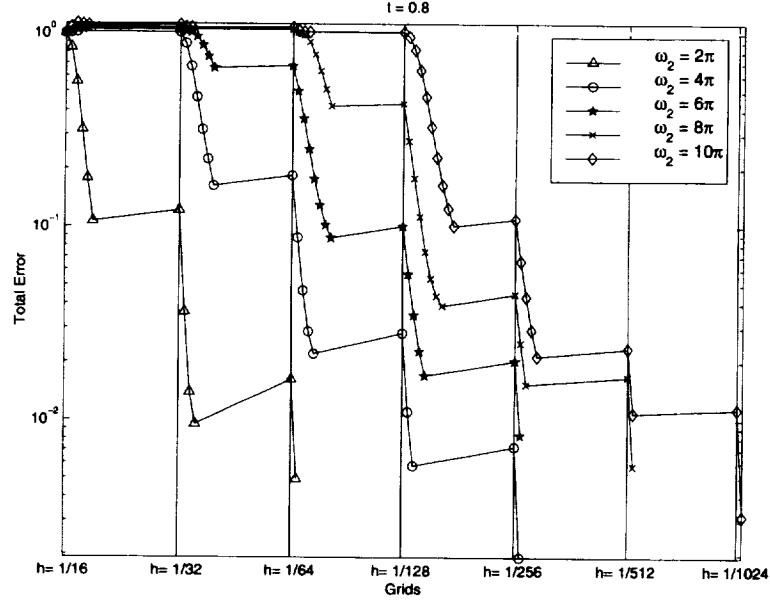


FIG. 4.1. DC1: Adaptive multigrid algorithm (DC1-AMA).

iterations. The input data were chosen so that the function $U(x, y) = \sin(\omega_2(y - tx))$ is the exact solution of (1.1), (1.3). The non-alignment parameter was set to $t = 0.8$. We tested different frequencies ω_2 providing a smooth solution to the problem with y -periodic boundary conditions for which the 1%-accurate solution can be obtained on a grid with $h \geq 2^{-9}$. The vertical coordinate on the figures marks (logarithm of) the total error and vertical lines separate the results corresponding to calculations on different grids. The first value on each grid (except the coarsest grid) is the value of the total error after the solution interpolation from the previous coarse grid. All the next values indicate the total error after the corresponding defect-correction iterations. The adaptive algorithm proved to be quite efficient requiring one extra level iteration at most to ascertain that the 1%-accuracy is already achieved. This is a very reasonable cost equal to the cost of few additional sweeps on the coarsest possible grid where the 1%-accuracy could be reached.

The small number of iterations performed by DC1-AMA on the fine grids does not disprove the claim that the number of required iterations might grow on the fine grids. The accuracy considerations make sense only for differentiable solution. The three solution conditions (the vertical periodicity, the 1%-accuracy on a grid with $h \geq 2^{-9}$ and the differentiability) together leave us just a few allowed components (only those with $\omega_2 = 2\pi k$, $k = 0, 1, 2, 3, 4, 5, 6$). Therefore, we have no chance to approach on the tested grids the $\bar{\omega}$ -component which realizes this predicted behavior. Of course, on finer grids the expected behavior is much likely to be manifested.

The efficiency of DC2-AMA seems to be nearly optimal.

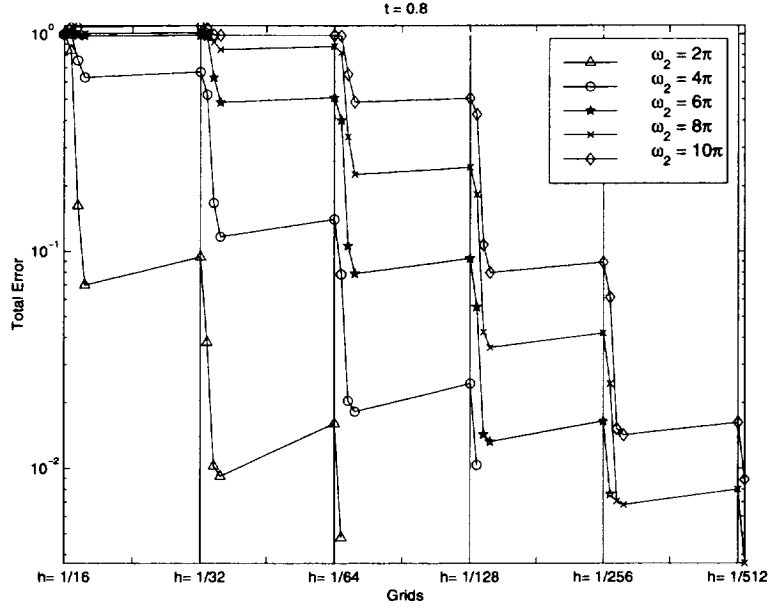


FIG. 4.2. DC2: Adaptive multigrid algorithm (DC2-AMA).

5. Conclusions. To summarize the practical results of the research reported in this paper we make the following conclusions:

1. The efficiency of the defect-correction method with the first order driver is grid dependent. The number of iterations required to reach the desired accuracy (or the asymptotic convergence rate regime) might grow on the fine grids (roughly as $h^{-\frac{1}{3}}$).
2. Using the second order driver in the defect-correction iterations eliminate this dependence resulting in a very efficient solver. We are aware that in many cases the choice of the first order driver is dictated by external reasons. For example, in solving discretized multidimensional hyperbolic systems of equations where downstream marching is impossible, first order schemes are considered to be much easier to solve than higher-order schemes. Nevertheless, we believe that even in such cases the opportunity of employing the second order driver should be carefully studied.
3. Any robust solver using defect-correction iterations should adopt the adaptive multigrid approach. Several further simplifications can be suggested on this way. For example, if the boundary conditions and/or the problem geometry prove to be too complicated, so that it seems hard to estimate N_{sweeps} on each grid, then the second criterion in Step 4 for stopping iterations on a given grid (performing all N_{sweeps} iterations) can be omitted. In many cases this results in some additional work on coarse grids but does not affect the total work count.
4. The discrete half-space analysis described in Sec. 2.1 is an accurate and very efficient tool for predicting actual solution behavior.
5. The defect-correction iterations converge residuals to the computer zero. The asymptotic convergence rate and an upper (but not the sharpest) bound can be calculated by means of the matrix analysis reported in Sec. 2.2

REFERENCES

- [1] S. A. ALLMARAS, *Multigrid for the 2D compressible navier-stokes equations*. Extended abstract for 14th AIAA CFD Conference, July 1999.
- [2] A. BRANDT, *Multigrid solvers for non-elliptic and singular-perturbation steady-state problems*. (unpublished). The Weizmann Institute of Science, Rehovot, Israel, December 1981.
- [3] ———, *The Weizmann Institute of Science research in multilevel computations:1988 report*, in Proc. 4th Copper Mountain Conf. on Multigrid Methods, Mandel, J. et al; ed., SIAM, 1989, pp. 13–53.
- [4] A. BRANDT AND I. YAVNEH, *On multigrid solution of high-Reynolds incompressible entering flow*, J. Comput. Phys., 101 (1992), pp. 151–164.
- [5] J. A. DESIDERI AND P. W. HEMKER, *Convergence analysis of the defect-correction iteration for hyperbolic problems*, SIAM J. Sci. Comp., 16 (1995), pp. 88–118.
- [6] P. W. H. K. BOHMER AND H. J. STETTER, *The defect correction approach*, in Defect Correction Methods, K. Bohmer, H. J. Stetter, ed., Comp. Suppl., 5, Wien, New York, Springer-Verlag, 1984, pp. 1–32.
- [7] N. YANENKO AND Y. SHOKIN, *Correctness of first differential approximations of difference schemes*, Dokl. Akad. Nauk SSSR, 182 (1968), pp. 776–778. (in Russian).

REPORT DOCUMENTATION PAGE			Form Approved OMB No. 0704-0188	
Public reporting burden for this collection of information is estimated to average 1 hour per response, including the time for reviewing instructions, searching existing data sources, gathering and maintaining the data needed, and completing and reviewing the collection of information. Send comments regarding this burden estimate or any other aspect of this collection of information, including suggestions for reducing this burden, to Washington Headquarters Services, Directorate for Information Operations and Reports, 1215 Jefferson Davis Highway, Suite 1204, Arlington, VA 22202-4302, and to the Office of Management and Budget, Paperwork Reduction Project (0704-0188), Washington, DC 20503.				
1. AGENCY USE ONLY (Leave blank)	2. REPORT DATE March 1999	3. REPORT TYPE AND DATES COVERED Contractor Report		
4. TITLE AND SUBTITLE Solving Upwind-biased Discretizations: Defect-correction Iterations			5. FUNDING NUMBERS C NAS1-97046 WU 505-90-52-01	
6. AUTHOR(S) Boris Diskin James L. Thomas				
7. PERFORMING ORGANIZATION NAME(S) AND ADDRESS(ES) Institute for Computer Applications in Science and Engineering Mail Stop 403, NASA Langley Research Center Hampton, VA 23681-2199			8. PERFORMING ORGANIZATION REPORT NUMBER ICASE Report No. 99-14	
9. SPONSORING/MONITORING AGENCY NAME(S) AND ADDRESS(ES) National Aeronautics and Space Administration Langley Research Center Hampton, VA 23681-2199			10. SPONSORING/MONITORING AGENCY REPORT NUMBER NASA/CR-1999-209106 ICASE Report No. 99-14	
11. SUPPLEMENTARY NOTES Langley Technical Monitor: Dennis M. Bushnell Final Report To be submitted to the SIAM Journal of Scientific Computing.				
12a. DISTRIBUTION/AVAILABILITY STATEMENT Unclassified-Unlimited Subject Category 64 Distribution: Nonstandard Availability: NASA-CASI (301) 621-0390			12b. DISTRIBUTION CODE	
13. ABSTRACT (Maximum 200 words) This paper considers defect-correction solvers for a second order upwind-biased discretization of the 2D convection equation. The following important features are reported (1) The asymptotic convergence rate is about 0.5 per defect-correction iteration. (2) If the operators involved in defect-correction iterations have different approximation order, then the initial convergence rates may be very slow. The number of iterations required to get into the asymptotic convergence regime might grow on fine grids as a negative power of h . In the case of a second order target operator and a first order driver operator, this number of iterations is roughly proportional to $h^{-1/3}$. (3) If both the operators have the second approximation order, the defect-correction solver demonstrates the asymptotic convergence rate after three iterations at most. The same three iterations are required to converge algebraic error below the truncation error level. A novel comprehensive half-space Fourier mode analysis (which, by the way, can take into account the influence of discretized outflow boundary conditions as well) for the defect-correction method is developed. This analysis explains many phenomena observed in solving non-elliptic equations and provides a close prediction of the actual solution behavior. It predicts the convergence rate for each iteration and the asymptotic convergence rate. As a result of this analysis, a new very efficient adaptive multigrid algorithm solving the discrete problem to within a given accuracy is proposed. Numerical simulations confirm the accuracy of the analysis and the efficiency of the proposed algorithm. The results of the numerical tests are reported.				
14. SUBJECT TERMS convection, upwind-biased discretization, defect-correction iteration			15. NUMBER OF PAGES 27	
			16. PRICE CODE A03	
17. SECURITY CLASSIFICATION OF REPORT Unclassified	18. SECURITY CLASSIFICATION OF THIS PAGE Unclassified	19. SECURITY CLASSIFICATION OF ABSTRACT	20. LIMITATION OF ABSTRACT	